ACS APPLIED MATERIALS & INTERFACES

Research Article

www.acsami.org

Bioactive Nanoparticle through Postmodification of Colloidal Silica

Chen Wang,[†,‡] Yue Xie,[†] Ailing Li,*[,†] Hong Shen,[†] Decheng Wu,[†] and Dong Qiu*[,†]

[†]Beijing National Laboratory for Molecular Sciences, State Key Laboratory of Polymer Physics and Chemistry, Institute of Chemistry, Chinese Academy of Sciences, Beijing 100190, China

[‡]University of Chinese Academy of Sciences, Beijing 100190, China

Supporting Information

ABSTRACT: Bioactive nanoparticles with controllable size and good colloidal stability were synthesized through surface modification of colloidal silica nanoparticles with $Ca(OH)_2$ as the modifier. These modified nanoparticles showed good bioactivity, showing evidence of hydroxyapatite formation when incubated in simulated body fluid within 3 days. Comparison of bioactivity was made among different sized particles from nanoscale to microscale. It was found the bioactivity of these calcium modified colloidal silica particles generally decreased with particle size in the explored size range (40 nm particles showed bioactivity within 1 day). These particles were also found to be noncytotoxic but promote preosteoblast growth, thus making them promising bioactive additives for bone repair materials.

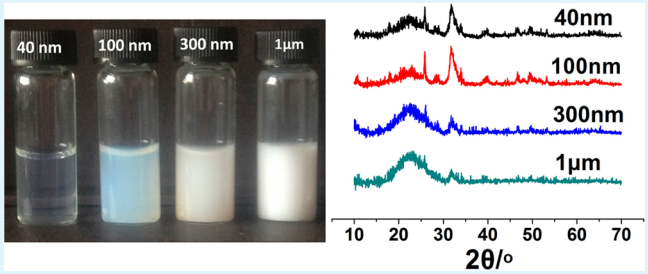

KEYWORDS: *Bioactive nanoparticle, colloidal silica, bioactivity, $Ca(OH)_2$, surface modification*

1. INTRODUCTION

Silica-based bioactive ceramics and glasses have been developed with remarkable biological features such as the ability to bond to bone and stimulate the growth of new bone.[1,2] Silica-based bioactive particles are one of the most important forms of silica-based bioactive ceramics and glasses in practical applications, because they are convenient to be pressed into the bone defects[3−5] or be blended with polymers for the improvement in bioactivity and mechanical strength.[6] Recently, nanosized instead of the conventional micrometer-sized bioactive particles have been used as fillers to polymers, with the expectation for better improvement in bioactivity and mechanical properties.[7,8] Larger specific surface area of the bioactive nanoparticles allows a faster release of ions and provides a larger interface for the reactant, accelerating the deposition of calcium and phosphate ions. Additionally, the size of bioactive nanoparticles is close to that of nanoscale hydroxyapatite (HA) crystallites (i.e., less than 100 nm in diameter),[7,9] which are the inorganic constituent of natural bone.

The most common way to produce nanosized bioactive particles is through the sol−gel process,[10−13] in which the most challenging part is to incorporate calcium into the composition through the sol−gel process. Calcium nitrate is the most commonly used precursor in the sol−gel preparation of bioactive glasses and ceramics,[12,14] which needs to be calcinated at above 500 °C to remove toxic nitrate ions.[15] Although the use of calcium methoxyethoxide as a calcium precursor can avoid such a high temperature treatment, still the organic moieties from the hydrolysis needs to be heated up to 200 °C, which is not ideal to keep the particles well dispersed.[16,17] Besides, the morphology of colloidal particles also becomes less controllable when calcium is in present,[10−13] preventing them from being used for precise structure−property relationship studies. Bioactive nanoparticles with mean diameters of 20 and 650 nm have been synthesized recently through sol−gel process; nevertheless, the size distributions were found to be rather broad for both sized samples.[11,12] A combination of the sol−gel and the coprecipitation method has also been tried to produce the ternary bioactive glass/ceramic nanoparticles. Unfortunately, although the size distribution of the particles was improved, the particle shape tended to be quite irregular.[13]

As summarized by Hench et al.,[18] the most significant stages during the formation of HA for bioactive silicate glasses in body fluid or simulated body fluid (SBF) are the creation of silanol (Si−OH) groups and release of calcium ions. Oversaturated Ca^{2+} released from bioactive glass will induce mineral precipitation from body fluid or SBF, which nucleates on silanol sites. Upon suitable physiochemical conditions (like those in body fluid or SBF), the precipitation is dominated by HA, thus being bioactive. Monodispersed spherical colloidal silica nanoparticles with abundant Si−OH groups on the surface can be readily fabricated through the sol−gel process. However, these colloidal silica nanoparticles do not show bioactivity (i.e., they do not promote the formation of HA on the surface when reacted with SBF or an equivalent), probably due to the lack of calcium ion release, which is essential for the formation of HA. Therefore, the incorporation of calcium ions

Received: December 25, 2013
Accepted: March 19, 2014
Published: March 19, 2014

   dx.doi.org/10.1021/am5014858 | ACS Appl. Mater. Interfaces 2014, 6, 4935−4939

into colloidal silica nanoparticles may be a feasible way to improve their bioactivity.

In the current work, $Ca(OH)_2$ was used to prepare monodispersed bioactive nanoparticles through postmodification of colloidal silica nanoparticles at room temperature. $Ca(OH)_2$ can break down Si−O−Si bondage through hydroxide groups, thus incorporating calcium into the silicate network, which can be then released when immersed in body fluid or SBF. The Si−OH groups on the surface of the colloidal silica particles (CSPs) provided sites for HA precipitation. The modification of CSPs by $Ca(OH)_2$ mainly took place on the particle surface; therefore, the size and size distribution of colloidal silica particles were well maintained, serving as good model systems for structure−property relationship studies.

2. MATERIALS AND METHODS

2.1. Synthesis of CSPs with Various Sizes. Monodispersed CSPs were synthesized through the well-known method developed by Stöber et al.[19] The size of the colloidal silica particles was tuned by varying the amounts of ammonium hydroxide and TEOS. The synthesis conditions and composition of the synthesis mixture are summarized in Table 1. The as-synthesized CSPs were collected by centrifugation and washed with absolute ethanol twice to remove unreacted precursors, then dispersed in water. All CSPs for the preparation of bioactive nanoparticles were in the form of aqueous colloidal dispersion and diluted with pure water before use. The CSPs with mean diameters of 40 nm, 100 nm, 300 nm and 1 μm were denoted as CSP-40, CSP-100, CSP-300 and CSP-1000, respectively.

Table 1. Recipes for the Synthesis of CSPs with Various Sizes

sample	ethanol/mL	NH_4OH/mL	TEOS/g	H_2O/mL
CSP-40	150.0	5.0	2.0	
CSP-100	215.7	3.7	10.4	20.0
CSP-300	223.0	18.7	8.9	7.1
CSP-1000	91.9	27.5	12.7	9.75

2.2. Synthesis of Bioactive Particles (BPs) with Various Sizes. Spherical BPs were synthesized by the surface modification on CSPs with $Ca(OH)_2$. Briefly, $Ca(OH)_2$ was added to the colloidal dispersion of CSPs prepared previously at a ratio of 1.5 mL $Ca(OH)_2$ (1 mmol·L^{-1}) to 2 mL CSPs (2.5 mg·mL^{-1}) and stirred for 12 h. The as-synthesized BPs were collected by centrifugation and washed with pure water to remove unreacted $Ca(OH)_2$. The bioactive particles prepared by the CSPs with mean diameters of 40 nm, 100 nm, 300 nm and 1 μm were denoted as BP-40, BP-100, BP-300 and BP-1000, respectively.

2.3. Characterizations. Transmission electron microscopy (TEM) micrographs were taken on a JEM 2011 with a 200 kV voltage. The dynamic light scattering results of BPs were collected using Zetasizer Nano. Powder X-ray diffraction (XRD) data were recorded on an Empyrean X-ray diffractometer using filtered Cu Kα radiation (λ) 1.5406 Å at 40 kV and 40 mA. Data were recorded by step scan with a step size of 0.026°/s. Fourier transform infrared spectroscopy (FTIR) measurements were performed on a Perkin-Elmer spectrum spotlight 200FTIR microscope system. For the MTT assay, the optical density (O.D.) values were measured using a Spectramax M5 microplate reader.

2.4. Bioactivity Test in Vitro. Bioactivity of the obtained particles was investigated by reacting with SBF at 36.5 °C, as suggested by previous studies.[20] Here 75 mg of nanoparticle powder was immersed in 50 mL of SBF and placed in a thermostatic water bath. The powder in SBF was isolated by centrifugation, washed with pure water and dried at ambient temperature under vacuum, at different intervals, then characterized by XRD and FTIR for HA formation .

2.5. Cell Toxicity. To evaluate the effect of BPs on the cell growth, the MTT assay was used.[21,22] For the assay, preosteoblast MC 3T3-E1 cells were incubated in the Dulbecco's modified Eagle medium (DMEM) supplemented with 10% fetal bovine serum (FBS), 0.1 mg·mL^{-1} penicillin and 0.1 mg·mL^{-1} streptomycin at a density of 5×10^3 cells per well. Gelatin was also included to mimic the cell growth in bone tissue, at a concentration of 3 mg·mL^{-1}. BPs (3 mg·mL^{-1}) were added to the culture media in which the cells had been seeded. To investigate the effect of SiO_2 on the cell growth, cells were also cultured in DMEM with CSPs. The cells incubated in DMEM without BPs, CSPs and gelatin were used as a control. All four groups were incubated under standard conditions. At different intervals, the culture medium was replaced with a serum-free medium containing thiazolyl blue (MTT) and incubated for 4 h at 37 °C in a humidified atmosphere of 5% CO_2. Dimethyl sulfoxide was added to dissolve the formazan crystals. The O.D. value of the supernatant solution was read at 490 nm after complete dissolution.

2.6. Statistics Analysis. The one-way analysis of variance (ANOVA) was used to evaluate significant differences between means in the measured data. Each experiment was repeated three times. All quantitative data were presented as mean ± standard deviation.

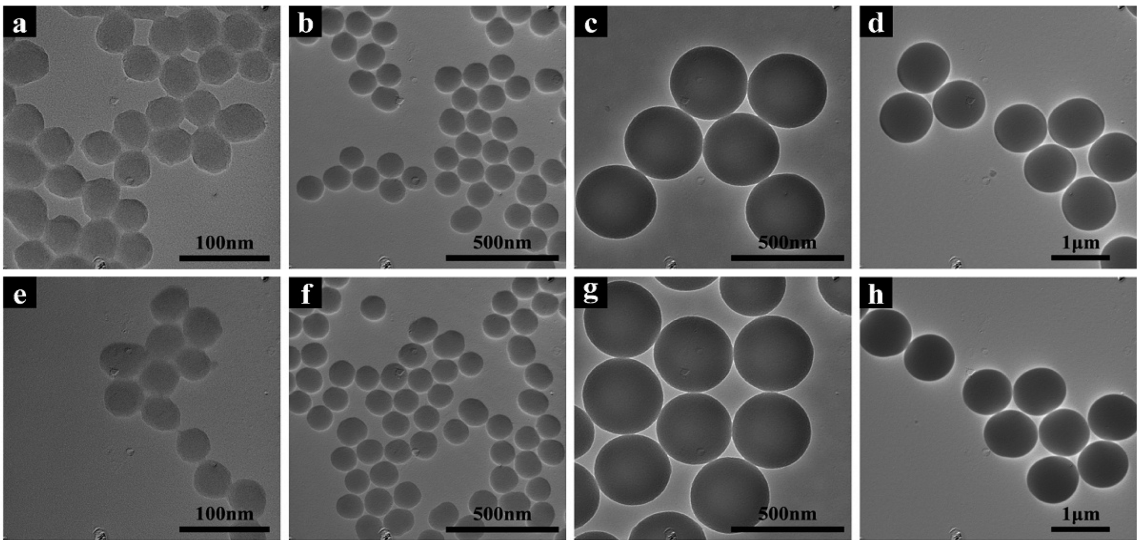

Figure 1. TEM images for CSPs: (a) 40 nm; (b) 100 nm; (c) 300 nm; (d) 1 μm. BPs: (e) 40 nm; (f) 100 nm; (g) 300 nm; (h) 1 μm.

3. RESULTS AND DISCUSSION

CSPs with abundant Si−OH groups on the surface were synthesized through the sol−gel process at room temperature. Figure 1 shows the typical TEM images of as-synthesized CSPs with different sizes. The spherical CSPs were monodisperse for all four samples (Figures 1a−d). As expected, the size of CSPs varied with the amount of TEOS and ammonium hydroxide used in the synthetic procedure. From TEM images, the average diameters of these CSPs were about 40 nm, 100 nm, 300 nm and 1 μm, respectively.

BPs were prepared by surface modification on CSPs by $Ca(OH)_2$. It was found that the size and morphology were well maintained after modification according to the TEM images (Figures 1e−h), in agreement with our hypothesis that the modification only takes place at particle surface.

Good colloidal stability is essential to ensure these particles distributing evenly when incorporated in a polymer matrix. It was found after surface modification that BPs still have good colloidal stabilities. BP-40 and BP-100 dispersions could be stored for more than 1 month without sedimentation at ambient conditions. The particle size and size distribution of BP-40 and BP-100 before and after storing were evaluated through dynamic light scattering (DLS) (Figure 2) (The sizes

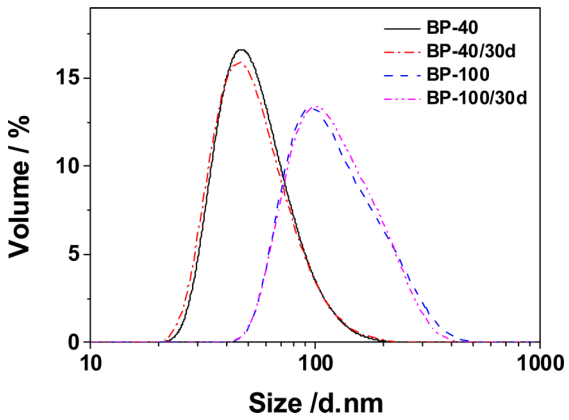

Figure 2. Size distribution profiles of BP-40 and BP-100 before and after storage for 30 days.

of BPs measured by DLS are somehow different from TEM results as DLS gives hydrodynamic sizes). After storage for 30 days, the particle size and size distribution nearly remained the same as those before storage, except for some negligible differences. The zeta potentials of BP-40 and BP-100 are also listed in Table 2. During the storage, the zeta potentials of BP-40 and BP-100 kept high values, demonstrating that these colloids were still potentially stable, in agreement with DLS results. However, for larger particle sizes, sedimentations may occur owing to gravity during the storage. In these cases, homogeneous dispersions were regained by ultrasonic for several minutes.

It has been well-established that it is the layer of bone-like apatite formed on the material surface that is responsible for the bonding between the material and surrounding bone. Accordingly, an essential requirement for the as-synthesized particles to be bioactive is the formation of a biologically active bone-like apatite on their surface when in contact with the physiological environment. This property can be evaluated in vitro by incubation in SBF.

CSPs and BPs were incubated in SBF for 1, 2, 3, 7, and 14 days. HA formation was first investigated by XRD. It was found that the CSPs were amorphous for all sizes, even after incubation for 14 days in SBF (Figure 3a), i.e., they are not

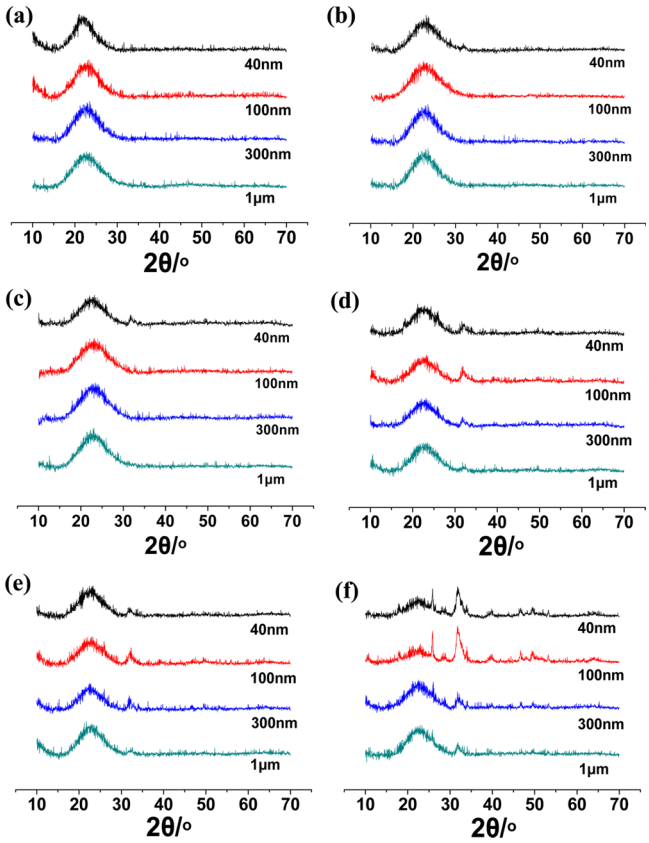

Figure 3. XRD spectra of CSPs incubated in SBF for 14 days (a) and BPs incubated in SBF for 1 (b), 2 (c), 3 (d), 7 (e) and 14 days (f).

bioactive. After reaction with SBF for 3 days, characteristic diffraction peaks corresponding to HA (25.88, 28.85, 31.70, 32.82, 39.69, 46.61, 49.43 and 53.20°) for BPs could be observed,[12,16] manifesting their good bioactivities (Figure 3d). Especially, for BP-40, the bioactivity was shown the earliest, after soaking in SBF for only 1 day (Figure 3b). When incubated for longer times in SBF, the intensity of the peaks from HA became stronger, showing further growth of HA (Figures 3e,f). BP-40 showed the highest bioactivity, as it formed HA within 1 day in SBF, which is very important for bone bonding at the early stage. It is a bit surprising that after 3 days, the intensity of HA peaks for BP-100 is higher than BP-40, which might be due to the size effect on crystallization

Table 2. Zeta Potential of BP-40 and BP-100

sample	BP-40[a]	BP-40/30d[b]	BP-100[a]	BP-100/30d[b]
zeta potential (mV)	−36.8 ± 3.1	−32.4 ± 1.6	−32.3 ± 1.9	−29.5 ± 2.7

[a]Samples freshly prepared. [b]Samples after storage for 30 days.

dx.doi.org/10.1021/am5014858 | ACS Appl. Mater. Interfaces 2014, 6, 4935−4939

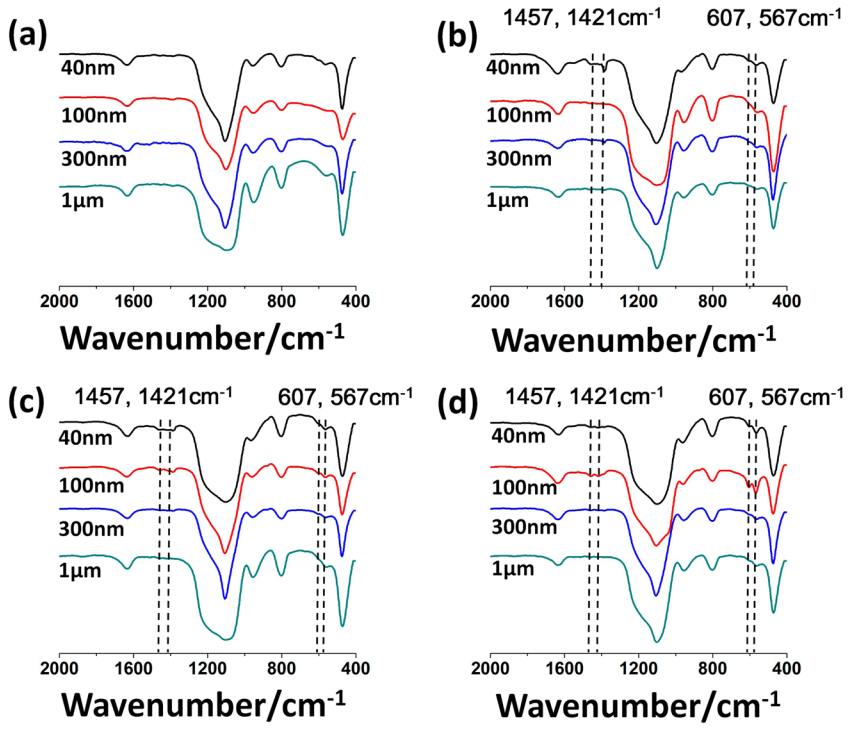

Figure 4. FTIR spectra of CSPs incubated in SBF for 14 days (a) and BPs incubated in SBF for 3 (b), 7 (c) and 14 days (d).

growth. Nevertheless, it is safe to conclude that the bioactivity of BPs generally decreased with particle size, i.e., nanosized BPs are more bioactive than micrometer-sized BPs, probably due to the decrease in their specific surface area, which again suggested that the calcium modification was most likely on the particle surface.

FTIR was also used to study the HA formation. The presence of double peaks at 607 and 567 cm^{-1} on the FTIR spectra could be the evidence of phosphate. FTIR showed that before $Ca(OH)_2$ modification, no phosphate was precipitated on these particles whereas, from 3 days on, the stretching vibration of phosphate groups became evitable (Figures 4a–c), especially after 14 days (Figure 4d), confirming the formation of apatite.[23] Meanwhile, the absorption bands of carbonate groups (1421, 1457, 1550 and 875 cm^{-1}) were also observed for BPs after reaction with SBF (Figures 4b–d), suggesting the formed HA might be carbonate substituted apatite (HCA), similar to that found in natural bones. Similar size effect as that found by XRD was also observed in FTIR studies, again supporting the key role of specific surface area.

The MTT assay was used to evaluate the biocompatibility of BPs. For the assay, preosteoblast MC 3T3-E1 cells, a nontransformed murine preosteoblastic cell line, were used. Preosteoblast MC 3T3-E1 cells had the capacity to differentiate into osteoblasts and osteocytes and were demonstrated to form calcified bone tissue in vitro. Thus, it was of great importance to test the toxicity effect on MC 3T3-E1 cells of BPs, which would be used as a bioactive composition to prepare bone repair materials. Cell viability values were all normalized to the control sample at the sample cell culture intervals, thus values greater than 100% mean good biocompatibility. BPs of 40 nm were chosen as they had the highest bioactivity, showing HA formation within 1 day in SBF. Figure 5 showed that BPs did not have any negative effect on the growth of the cells, indicating they had no toxicity on preosteoblast MC 3T3-E1

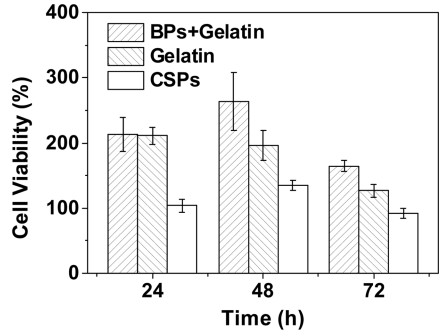

Figure 5. MTT assay for proliferation of preosteoblast MC 3T3-E1 cells.

cells. Indeed, the group with BPs even showed a better performance on the acceleration of the cell growth than the other three groups within the incubation time, further confirming their good bioactivity. It is interesting to see that the cell viability values were high at the beginning, then eventually approached 100%. This is not surprising because it was demonstrated that the dissolution of bioactive glass could promote osteoblast growth,[24] while the dissolution concentration will inevitably decrease as HA covers BP surface.

BP-40 and CSP-40 were also made into composites scaffolds with gelatin to mimic the porous structure of the bone tissue. Preosteoblast MC 3T3-E1 cells were seeded on the scaffolds and cultured for 2 days. Much more cells were found to adhere to the scaffold composited with BP-40 (Figure S1a, Supporting Information) than the scaffold with CSPs and the scaffold without either particle (Figure S1b,c, Supporting Information). Thus, the addition of BPs into the composite enhanced the osteogenic differentiation.

dx.doi.org/10.1021/am5014858 | ACS Appl. Mater. Interfaces 2014, 6, 4935–4939

4. CONCLUSION

In summary, we have succeeded in the synthesis of BPs with well controlled size and size distribution through post-modification of CSPs by $Ca(OH)_2$. The BPs showed good bioactivity with HCA formed upon reaction with SBF within 3 days. The bioactivity of BPs was found to generally increase with decreasing particle size, probably due to the increase in specific surface area. Additionally, the BPs showed no cytotoxicity on preosteoblasts as suggested by MTT assay tests, making them promising bioactive additives for bone repair materials.

■ ASSOCIATED CONTENT

Supporting Information

Confocal fluorescent microscopy images of MC3T3-E1 preosteoblast cells cultured on the BPs/gelatin scaffolds This material is available free of charge via the Internet at http://pubs.acs.org.

■ AUTHOR INFORMATION

Corresponding Authors

* Ailing Li. E-mail: liailing@iccas.ac.cn.
* Dong Qiu. E-mail: dqiu@iccas.ac.cn.

Notes

The authors declare no competing financial interest.

■ ACKNOWLEDGMENTS

This work was supported by MOST (Project No. 2012CB933200, 2013DFG52300-1) and NSFC (Project No. 51173193, 81202931).

■ REFERENCES

(1) Hench, L. L.; Wilson, J. Surface-Active Biomaterials. *Science* **1984**, *226*, 630−636.
(2) Hench, L. L.; Polak, J. M. Third-Generation Biomedical Materials. *Science* **2002**, *295*, 1014−1017.
(3) Schepers, E. J.; Ducheyne, P.; Barbier, L.; Schepers, S. Bioactive Glass Particles of Narrow Size Range: A New Material for the Repair of Bone Defects. *Implant Dent.* **1993**, *2*, 151−156.
(4) Turunen, T.; Peltola, J.; Yli-Urpo, A.; Happonen, R. P. Bioactive Glass Granules as A Bone Adjunctive Material in Maxillary Sinus Floor Augmentation. *Clin. Oral Implants Res.* **2004**, *15*, 135−141.
(5) Waltimo, T.; Mohn, D.; Paqué, F.; Brunner, T. L.; Stark, W. J.; Imfeld, T.; Schätzle, M.; Zehnder, M. Fine-Tuning of Bioactive Glass for Root Canal Disinfection. *J. Dent. Res.* **2009**, *88*, 235−238.
(6) Gentile, P.; Mattioli-Belmonte, M.; Chiono, V.; Ferretti, C.; Baino, F.; Tonda-Turo, C.; Vitale-Brovarone, C.; Pashkuleva, I.; Reis, R. L.; Ciardelli, G. Bioactive Glass/Polymer Composite Scaffolds Mimicking Bone Tissue. *J. Biomed. Mater. Res., Part A* **2012**, *100*, 2654−2667.
(7) Caridade, S. G.; Merino, E. G.; Alves, N. M.; de Zea Bermudez, V.; Boccaccini, A. R.; Mano, J. F. Chitosan Membranes Containing Micro or Nano-Size Bioactive Glass Particles: Evolution of Biomineralization Followed by in Situ Dynamic Mechanical Analysis. *J. Mech. Behav. Biomed. Mater.* **2013**, *20*, 173−183.
(8) Tamjid, E.; Bagheri, R.; Vossoughi, M.; Simchi, A. Effect of Particle Size on the in Vitro Bioactivity, Hydrophilicity and Mechanical Properties of Bioactive Glass-Reinforced Polycaprolactone Composites. *Mater. Sci. Eng., C* **2011**, *31*, 1526−1533.
(9) Kay, S.; Thapa, A.; Haberstroh, K. M.; Webster, T. J. Nanostructured Polymer/Nanophase Ceramic Composites Enhance Osteoblast and Chondrocyte Adhesion. *Tissue Eng.* **2002**, *8*, 753−761.
(10) Mozafari, M.; Rabiee, M.; Azami, M.; Maleknia, S. Biomimetic Formation of Apatite on the Surface of Porous Gelatin/Bioactive Glass Nanocomposite Scaffolds. *Appl. Surf. Sci.* **2010**, *257*, 1740−1749.
(11) Curtis, A. R.; West, N. X.; Su, B. Synthesis of Nanobioglass and Formation of Apatite Rods to Occlude Exposed Dentine Tubules and Eliminate Hypersensitivity. *Acta Biomater.* **2010**, *6*, 3740−3746.
(12) Lin, S.; Ionescu, C.; Pike, K. J.; Smith, M. E.; Jones, J. R. Nanostructure Evolution and Calcium Distribution in Sol−Gel Derived Bioactive Glass. *J. Mater. Chem.* **2009**, *19*, 1276−1282.
(13) Hong, Z.; Liu, A.; Chen, L.; Chen, X.; Jing, X. Mono-dispersed Bioactive Glass Nanospheres: Preparation and Effects on Biomechanics of Mammalian Cells. *J. Non-Cryst. Solids* **2009**, *355*, 368−372.
(14) Skipper, L. J.; Sowrey, F. E.; Pickup, D. M.; Drake, K. O.; Smith, M. E.; Saravanapavan, P.; Hench, L. L.; Newport, R. J. The Structure of a Bioactive Calcia-Silica Sol-gel Glass. *J. Mater. Chem.* **2005**, *15*, 2369−2374.
(15) Jones, J. R.; Ehrenfried, L. M.; Hench, L. L. Optimising Bioactive Glass Scaffolds for Bone Tissue Engineering. *Biomaterials* **2006**, *27*, 964−973.
(16) Yu, B.; Turdean-Ionescu, C. A.; Martin, R. A.; Newport, R. J.; Hanna, J. V.; Smith, M. E.; Jones, J. R. Effect of Calcium Source on Structure and Properties of Sol−Gel Derived Bioactive Glasses. *Langmuir* **2012**, *28*, 17465−17476.
(17) Sun, Y.; Li, A.; Xu, F.; Qiu, D. A Low-temperature Sol−Gel Route for the Synthesis of Bioactive Calcium Silicates. *Chin. Chem. Lett.* **2013**, *24*, 170−172.
(18) Hench, L. L. The Story of Bioglass. *J. Mater. Sci.: Mater. Med.* **2006**, *17*, 967−978.
(19) Stöber, W.; Fink, A.; Bohn, E. Controlled Growth of Monodisperse Silica Spheres in the Micron Size Range. *J. Colloid Interface Sci.* **1968**, *26*, 62−69.
(20) Lei, B.; Shin, K. H.; Noh, D. Y.; Jo, I. H.; Koh, Y. H.; Choi, W. Y.; Kim, H. E. Nanofibrous Gelatin−Silica Hybrid Scaffolds Mimicking the Native Extracellular Matrix (ECM) Using Thermally Induced Phase Separation. *J. Mater. Chem.* **2012**, *22*, 14133−14140.
(21) Jithendra, P.; Rajam, A. M.; Kalaivani, T.; Mandal, A. B.; Rose, C. Preparation and Characterization of Aloe Vera Blended Collagen-Chitosan Composite Scaffold for Tissue Engineering Applications. *ACS Appl. Mater. Interfaces* **2013**, *5*, 7291−7298.
(22) Nagiah, N.; Madhavi, L.; Anitha, R.; Anandan, C.; Srinivasan, N. T.; Sivagnanam, U. T. Development and Characterization of Coaxially Electrospun Gelatin Coated Poly (3-hydroxybutyric acid) Thin Films as Potential Scaffolds for Skin Regeneration. *Mater. Sci. Eng., C* **2013**, *33*, 4444−4452.
(23) Chen, X.; Meng, Y.; Li, Y.; Zhao, N. Investigation on Biomineralization of Melt and Sol−Gel Derived Bioactive Glasses. *Appl. Surf. Sci.* **2008**, *255*, 562−564.
(24) Xynos, I. D.; Hukkanen, M. V. J.; Batten, J. J.; Buttery, L. D.; Hench, L. L.; Polak, J. M. Bioglass®45S5 Stimulates Osteoblast Turnover and Enhances Bone Formation in Vitro: Implications and Applications for Bone Tissue Engineering. *Calcif. Tissue Int.* **2000**, *67*, 321−329.